α-ketoglutarate protects against septic cardiomyopathy by improving mitochondrial mitophagy and fission

WEI WU[1], QIONG MA[1], BO-TAO LI[1], SHUANG SHI[1], GONG-CHANG GUAN[1], JUN-KUI WANG[1], BAO-YAO XUE[2] and ZHONG-WEI LIU[1]

[1]Department of Cardiovascular Medicine, Shaanxi Provincial People's Hospital, Xi'an, Shaanxi 710068, P.R. China; [2]Department of Maternity, Shaanxi Provincial People's Hospital, Xi'an, Shaanxi 710068, P.R. China

Received November 8, 2024; Accepted March 14, 2025

DOI: 10.3892/mmr.2025.13511

Abstract. Septic cardiomyopathy is a considerable complication in sepsis, which has high mortality rates and an incompletely understood pathophysiology, which hinders the development of effective treatments. α-ketoglutarate (AKG), a component of the tricarboxylic acid cycle, serves a role in cellular metabolic regulation. The present study delved into the therapeutic potential and underlying mechanisms of AKG in ameliorating septic cardiomyopathy. A mouse model of sepsis was generated and treated with AKG via the drinking water. Cardiac function was assessed using echocardiography, while the mitochondrial ultrastructure was examined using transmission electron microscopy. Additionally, *in vitro*, rat neonatal ventricular myocytes were treated with lipopolysaccharide (LPS) as a model of sepsis and then treated with AKG. Mitochondrial function was evaluated via ATP production and Seahorse assays. Additionally, the levels of reactive oxygen species were determined using dihydroethidium and chloromethyl derivative CM-H_2DCFDA staining, apoptosis was assessed using a TUNEL assay, and the expression levels of mitochondria-associated proteins were analyzed by western blotting. Mice subjected to LPS treatment exhibited compromised cardiac function, reflected by elevated levels of atrial natriuretic peptide, B-type natriuretic peptide and β-myosin heavy chain. These mice also exhibited pronounced mitochondrial morphological disruptions and dysfunction in myocardial tissues; treatment with AKG ameliorated these changes. AKG restored cardiac function, reduced mitochondrial damage and corrected mitochondrial dysfunction. This was achieved primarily through increasing mitophagy and mitochondrial fission. *In vitro*, AKG reversed LPS-induced cardiomyocyte apoptosis and dysregulation of mitochondrial energy metabolism by increasing mitophagy and fission. These results revealed that AKG administration mitigated cardiac dysfunction in septic cardiomyopathy by promoting the clearance of damaged mitochondria by increasing mitophagy and fission, underscoring its therapeutic potential in this context.

Correspondence to: Dr Bao-Yao Xue, Department of Maternity, Shaanxi Provincial People's Hospital, 256 Youyi West Road, Beilin, Xi'an, Shaanxi 710068, P.R. China
E-mail: 18591088733@163.com

Dr Zhong-Wei Liu, Department of Cardiovascular Medicine, Shaanxi Provincial People's Hospital, 256 Youyi West Road, Beilin, Xi'an, Shaanxi 710068, P.R. China
E-mail: liuzhongwei@nwpu.edu.cn

Abbreviations: AKG, α-ketoglutarate; Bnip3, BCL2 interacting protein 3; MT-ND1, mitochondrial NADH-ubiquinone oxidoreductase chain 1; DRP1, dynamin-related protein 1; HIF-1α, hypoxia inducible factor-1α; OGDH, ketoglutarate dehydrogenase; PDH, pyruvate dehydrogenase; SDHA, succinate dehydrogenase; LPS, lipopolysaccharide; OXPHOS, oxidative phosphorylation; ROS, reactive oxygen species; LV, left ventricle; LVEDD, left ventricular end-diastolic dimension; LVESD, left ventricular end-systolic dimension; ANP, atrial natriuretic protein; BNP, brain natriuretic peptide; β-MHC, β-major histocompatibility complex; Ndufa12, NADH dehydrogenase (ubiquinone) 1α subcomplex subunit 12; Ndufab1, NADH:ubiquinone oxidoreductase subunit AB1; NOX2, NADPH oxidase 2; TEM, transmission electron microscopy; DHE, dihydroethidium; DCF, chloromethyl derivative CM-H2DCFDA; MDA, malondialdehyde; NRVM, neonatal rat ventricular myocyte

Key words: septic cardiomyopathy, AKG, mitochondria, mitophagy, fission

Introduction

Sepsis is a systemic inflammatory response secondary to infection, and is the leading cause of mortality in intensive care units, predominantly due to septic shock (1). Sepsis affects >3 million individuals worldwide annually (2). Septic cardiomyopathy, characterized by reduced left ventricular systolic and diastolic functions (3,4), is a considerable and fatal complication of sepsis, with mortality rates ranging between 40 and 50% (5,6). Despite extensive research identifying apoptosis, oxidative stress, inflammation and calcium signaling as key factors (5,7,8), the precise pathophysiological mechanisms underlying septic cardiomyopathy remain incompletely understood. This gap in understanding hampers the development of targeted therapeutics for this condition (9,10).

Mitochondria constitute the most voluminous organelles within cardiomyocytes, representing ~35% of the total cardiomyocyte volume (11). Mitochondria are implicated in septic

cardiomyopathy, serving as the primary targets of cellular damage (12). The primary role of mitochondria lies in ATP generation through oxidative phosphorylation (OXPHOS), which is the central energy source for cardiomyocytes (13). Furthermore, the production of reactive oxygen species (ROS) and the induction of apoptosis are intrinsically linked to mitochondrial function (14,15). Mitochondrial integrity and efficiency are maintained by a robust quality control system encompassing biosynthesis, fission, fusion and mitophagy (11). Dysfunctional mitochondria exhibit a compromised aerobic oxidation capacity and a reliance on glycolysis, culminating in an inadequate energy supply and consequent cardiac dysfunction (16). Additionally, mitochondrial damage is often associated with increased levels of ROS, and ROS signaling is a key factor in the pathogenesis of septic cardiomyopathy (5).

α-ketoglutarate (AKG), an intermediary in the tricarboxylic acid (TCA) cycle, is instrumental in the adaptation of cellular metabolism (17). AKG is involved in numerous metabolic processes, including the biosynthesis of amino acids, nucleotides, lipids and carnitine (18). Beyond its role in energy metabolism, AKG is involved in maintaining mitochondrial homeostasis, exerting antioxidant and anti-inflammatory effects, and promoting cellular proliferation (19,20). Notably, AKG has been demonstrated to enhance energy supplementation and mitigate oxidative stress during surgical procedures, as indicated by the levels of oxidatively modified proteins (21). In animal models of diabetic cardiomyopathy and pressure overload cardiomyopathy, AKG has been demonstrated to exert effective cardioprotective effects by ameliorating cardiac remodeling and improving cardiac function (22,23). However, to the best of our knowledge, the specific impact of AKG in the context of septic cardiomyopathy remains to be elucidated.

While the mechanisms underlying mitochondrial damage have been investigated in various forms of cardiomyopathy, such as dilated cardiomyopathy (24), takotsubo cardiomyopathy (25) and cardiomyopathy induced by antitumor drugs (26), their relevance in septic cardiomyopathy remains largely unexplored. To address this, cardiomyocytes and animal models of septic cardiomyopathy induced by lipopolysaccharide (LPS), a constituent of Gram-negative bacterial cell membranes (27), were used in the present study. Echocardiography was employed to assess cardiac function. For the examination of mitochondrial ultrastructure, transmission electron microscopy was utilized. The evaluation of mitochondrial function was carried out by means of ATP production assays and Seahorse assays. Moreover, the levels of reactive oxygen species were measured through staining with dihydroethidium and the chloromethyl derivative CM-H2DCFDA. The assessment of apoptosis was conducted using a TUNEL assay. Additionally, western blotting was used to analyze the expression of mitochondrial-associated proteins.

Materials and methods

Animals and treatment. Approval for the present study was obtained from the Shaanxi Provincial People's Hospital Ethics Committee (Xi'an, China) and the present study adhered to the National Institutes of Health's Guide for the Care and Use of Laboratory Animals (28). In the present study, a total of 32 male C57BL/6 mice (age, 8 weeks; weight, 18-22 g), obtained from GemPharmatech Co. Ltd., were acclimated for 1 week at a temperature of 25˚C, 55% humidity with a 12 h light/dark cycle and *ad libitum* access to food and water.

The mice were randomly divided into four groups (n=8/group). The two groups received a single intraperitoneal injection of LPS (10 mg/kg; MilliporeSigma) dissolved in PBS, to establish a model of septic cardiomyopathy (29). The remaining groups were pre-treated with 2% AKG (MilliporeSigma) in the drinking water for 9 weeks prior to LPS administration (23). Animals were anesthetized by isoflurane inhalation (4% induction and 2% maintenance), blood samples were collected by cardiac puncture, and then cardiac tissue was collected following cervical dislocation.

Echocardiography. Cardiac function was evaluated by transthoracic echocardiography using a Vevo 2100 ultrasound system (VisualSonics, Inc.) equipped with an MS550D transducer, as described previously (25). For imaging, 2D images of the left ventricle (LV) were captured at the papillary muscle level. M-mode tracings, encompassing both the anterior and posterior LV walls, were subsequently recorded. Key parameters, including LV end-diastolic dimension (LVEDD), LV end-systolic dimension (LVESD), ejection fraction and fractional shortening, were measured in a blinded manner. These measurements were derived from an average of five cardiac cycles to ensure accuracy and reliability.

Western blotting. Western blotting was performed as described previously (24). Following protein transfer, polyvinylidene fluoride membranes were blocked using 5% non-fat milk for 1 h at room temperature. This was followed by an overnight incubation at 4˚C with primary antibodies against atrial natriuretic protein (ANP; cat. no. ab225844; 1:500; Abcam), brain natriuretic peptide (BNP; cat. no. ab239510; 1:1,000; Abcam), β-major histocompatibility complex (β-MHC; cat. no. ab172967; 1:1,000; Abcam), BCL2 interacting protein 3 (Bnip3; cat. no. ab10433; 1:1,000; Abcam), LC3 (cat. no. 4599S; 1:1,000; Cell Signaling Technology, Inc.), Fis1 (cat. no. ab71498; 1:1,000; Abcam), dynamin-related protein 1 (DRP1; cat. no. 8570S; 1:1,000; Cell Signaling Technology, Inc.), NADH dehydrogenase (ubiquinone) 1α subcomplex subunit 12 (Ndufa12; cat. no. ab192617; 1:4,000; Abcam), NADH:ubiquinone oxidoreductase subunit AB1 (Ndufab1; cat. no. ab181021; 1:1,000; Abcam), mitochondrial NADH-ubiquinone oxidoreductase chain 1 (MT-ND1; cat. no. ab181848; 1:5,000; Abcam), succinate dehydrogenase (SDHA; cat. no. 11998; 1:4,000; Cell Signaling Technology, Inc.), complex IV (COX IV; cat. no. 11242-1-AP; 1:3,000; Proteintech Group, Inc.), oxoglutarate dehydrogenase (OGDH; cat. no. ab137773; 1:5,000; Abcam), pyruvate dehydrogenase (PDH; cat. no. 3205; 1:3,000; Cell Signaling Technology, Inc.), hypoxia inducible factor-1α (HIF-1α; cat. no. 36169; 1:1,000; Cell Signaling Technology, Inc.), NADPH oxidase 2 (NOX2; cat. no. bs-3889R; 1:1,000; BIOSS), NOX4 (cat. no. bs-1091R; 1:1,000; BIOSS), Bax (cat. no. 2772S; 1:3,000; Cell Signaling Technology, Inc.) and Bcl-2 (cat. no. 3498S; 1:1,000; Cell Signaling Technology, Inc.), GAPDH (cat. no. 10494-1-AP; 1:8,000; Proteintech Group, Inc.), α-tubulin (cat. no. 11224-1-AP; 1:4,000; Proteintech Group, Inc.) and HSP90 (cat. no. 11224-1-AP; 1:2,000; Proteintech Group,

Inc.). Following incubation with the primary antibody, the membranes were treated with horseradish peroxidase-conjugated secondary antibodies (anti-Mouse secondary antibodies; cat. no. 62-6520; 1:10,000; Thermo Fisher Scientific, Inc. and anti-Rabbit secondary antibodies; cat. no. VJ313046; 1:10,000; Thermo Fisher Scientific, Inc.) for 1 h at room temperature. Signals were visualized using Clarity™ Western ECL Substrate (Bio-Rad Laboratories, Inc.). Densitometry analysis was performed using ImageJ software (version 4.5.2; National Institutes of Health).

Reverse transcription-quantitative PCR (RT-qPCR). Total RNA was isolated from LV myocardial tissues using TRIzol® reagent (Invitrogen; Thermo Fisher Scientific, Inc.). From the extracted RNA, 1 μg was reverse-transcribed into cDNA using a RT kit (cat. no. RR047A; Takara Bio, Inc.) at 37˚C for 15 min and 85˚C for 5 sec. qPCR was performed using TB Green™ Premix Ex Taq™ II (Tli RNaseH Plus; cat. no. RR820A; Takara Bio, Inc.) on a Bio-Rad CFX96 Real-time PCR Detection System (Bio-Rad Laboratories, Inc.). The amplification protocol involved an initial denaturation at 95˚C for 30 sec, followed by 40 cycles of denaturation at 95˚C for 5 sec and annealing/extension at 60˚C for 30 sec. Gene expression levels were quantified relative to the housekeeping gene GAPDH for normalization using the $2^{-\Delta\Delta Cq}$ method (30). The sequences of the primers used for qPCR were: ANP forward, 5'-AAGAACCTGCTAGACCACCTGGAG-3' and reverse, 5'-TGCTTCCTCAGTCTGCTCACTCAG-3'; BNP forward, 5'-GGAAGTCCTAGCCAGTCTCCAGAG-3' and reverse, 5'-GCCTTGGTCCTTCAAGAGCTGTC-3'; β-MHC forward, 5'-CAGAACACCAGCCTCATCAACCAG-3' and reverse, 5'-TTCTCCTCTGCGTTCCTACACTCC-3'; and GAPDH forward, 5'-AGGTCGGTGTGAACGGATTTG-3' and reverse, 5'-TGTAGACCATGTAGTTGAGGTCA-3'.

Histological analysis. TUNEL staining of the LV tissue sections was performed according to the manufacturer's protocol. Briefly, heart tissues were fixed in 4% paraformaldehyde at room temperature overnight. Subsequently, tissues were embedded in paraffin and cut into slices with a thickness of 4 μm. After dewaxing and hydration, slices were stained with TUNEL reagent (cat. no. C1088; Beyotime Institute of Biotechnology) at room temperature for 1 h. Then, antifade mounting medium with DAPI (cat. no. P0131; Beyotime Institute of Biotechnology) solution was incubated at room temperature for 10 min for nuclear counterstaining. TUNEL-stained sections were imaged using an Olympus DP-72 fluorescence microscope (Olympus Corporation), focusing on the identification of apoptotic cells within the myocardium. Images were analyzed using ImageJ. The number of cardiomyocyte nuclei exhibiting green fluorescence (indicating apoptosis) was counted. To ensure objectivity, all analyses were carried out under double-blinded conditions. For each histological section, five random visual fields were selected for measurement. The average value from these fields was then used for statistical analysis.

Transmission electron microscopy (TEM) analysis. TEM was carried out as described previously (24). Fresh apical myocardial tissue from the LV was first fixed using 2.5% glutaraldehyde at 4˚C for 2 h. After fixation, a graded series of ethanol/acetone solutions was employed for dehydration, with the final solution being absolute acetone. The dehydrated samples were then infiltrated with Epon 812 resin. Ultrathin sections of the embedded tissues were prepared using an ultramicrotome (LKB-V/NOVA; Leica Microsystems GmbH) and stained with acidified uranyl acetate for enhanced contrast. Observation of the prepared samples was carried out using a Hitachi Model H-7650 TEM (Hitachi, Ltd.). ImageJ was used for quantitative analysis of the TEM images. Specifically, the count of mitochondria was determined from five images at a magnification of x10,000 per LV sample. Additionally, the proportion of mitochondria exhibiting structural impairments, such as incomplete outer membranes or dissolved cristae, was assessed from another set of five images at a magnification of x30,000 per LV sample. The count of aberrant mitochondria is presented as a percentage of the total mitochondrial count.

Determination of ROS levels. ROS levels in myocardial tissues were quantified using two distinct methods as described previously (24). Initially, O^{2-} content was assessed using 5-μm frozen myocardial sections. These sections were incubated with dihydroethidium (DHE; 5 μM) for 1 h at 37˚C. Fluorescence images were captured at a magnification of x400 (five fields per heart) using an Olympus DP-72 fluorescence microscope (Olympus Corporation), with excitation and emission wavelengths set at 488 and 610 nm, respectively. In the second method, cardiomyocytes were isolated via enzyme digestion using the Langendorff perfusion system. Briefly, the aorta was retrogradely perfused with collagenase II (cat. no. LS004177; Worthington Biochemical Corporation) at room temperature for 15 min to digest the heart. Subsequently, the heart was minced into small pieces and centrifuged at 1,400 x g for 3 min at room temperature. Finally, the isolated cardiomyocytes were transferred onto the cell culture dish. The isolated cells were then incubated with chloromethyl derivative CM-H_2DCFDA (DCF; 5 μM) for 30 min at 37˚C. Fluorescence imaging was performed using a Leica TCS SP8 STED 3X confocal microscope (Leica Microsystems GmbH), with a x40 1.3 NA oil immersion objective lens, with excitation at 488 nm and emission at 525 nm, using standardized scanning parameters. The intensity of DCF fluorescence was quantified using ImageJ, with an average of 80 cells analyzed per heart.

H&E staining. Briefly, the heart was fixed in 4% paraformaldehyde at room temperature overnight. Subsequently, it was embedded in paraffin and sliced into 4 μm slices. After deparaffinization and hydration, heart sections were stained with hematoxylin for 5 min and eosin for 1 min at room temperature using the H&E Staining kit (cat. no. 0105; Beyotime Institute of Biotechnology). The fluorescence images were captured using an Olympus DP-72 fluorescence microscope (Olympus Corporation) from 3-5 random fields.

ATP, lactate and malondialdehyde (MDA) assay. Fresh LV tissue and plasma was harvested to determine the content of ATP, lactate and MDA using commercial kits. ATP kits (cat. no. A095-2-1; Nanjing Jiancheng Bioengineering Institute), lactate kits (cat. no. E-BC-Ko44-M; Wuhan Elabscience

Biotechnology Co., Ltd.) and MDA kits (cat. no. R21869; Shanghai Yuanye Biotechnology Co., Ltd.) were carried out according to the manufacturer's protocol as described previously (25).

Measurement of circulating AKG content. Plasma levels of AKG were quantified using a commercial kit (cat. no. G0861W; Grace Biotech Co., Ltd.) according to the manufacturer's protocol.

Isolation and culture of neonatal rat ventricular myocytes (NRVMs). A total of 24 Neonatal Sprague-Dawley rats (age, 1-2 days; weight, 6-7 g) were purchased from the Laboratory Animal Center of Xi'an Jiaotong University (Xi'an, China), and humanely euthanized via cervical dislocation. Subsequently, their hearts were excised and subjected to enzymatic digestion using 1 ml 0.2% collagenase II for 5-6 min at 37˚C for six cycles. The digested tissue was centrifuged at 2,200 x g for 5 min at room temperature and the resultant cardiomyocytes were resuspended in F12 medium (Thermo Fisher Scientific, Inc.) supplemented with 15% FBS (Thermo Fisher Scientific, Inc.). This suspension was incubated for 60 min at 37˚C to facilitate differential adhesion, allowing for the separation of cardiomyocytes from non-myocyte cells. To further purify the culture, the cardiomyocytes were then treated with 5-bromo-2-deoxyuridine, an agent used to inhibit the proliferation of non-cardiomyocyte cells (31). After a 48-h incubation period at 37˚C, the NRVMs given the following treatments (Control, 2 mM AKG, 0.5 μg/ml LPS or a combination of 2 mM AKG and 0.5 μg/ml LPS) were used for TUNEL staining, western blotting and Seahorse assays. The control group was treated with F12 medium containing 10% FBS. These treatments were administered in F12 medium containing 10% FBS for a duration of 24 h at 37˚C as previously described (7,23).

Seahorse assay. The respiratory capacity of mitochondria in NRVMs was evaluated using the Agilent Seahorse XF24 Extracellular Flux Analyzer (Agilent Technologies, Inc.). NRVMs were initially seeded onto Seahorse XF24 cell culture microplates and subjected to the aforementioned treatments. The Seahorse XF sensor cartridge was prepared by hydrating its probe plate with calibration solution in a CO_2-free incubator maintained at 37˚C overnight. Subsequently, during the assay, specific mitochondrial inhibitors were sequentially added to the wells: Oligomycin A (1.5 μM; cat. no. 103672-100; Agilent) to inhibit ATP synthase, trifluoromethoxy carbonylcyanide phenylhydrazone (1 μM; cat. no. 103672-100; Agilent) to uncouple the proton gradient and antimycin A (0.5 μM; cat. no. 103672-100; Agilent) to inhibit the mitochondrial respiratory chain. The oxygen consumption rate, a key indicator of mitochondrial respiration, was measured following these additions, according to the manufacturer's protocol.

Statistical analysis. Data are presented as the mean ± standard error of the mean (n=6-8 repeats/group). To determine the normality and homogeneity of variance of the data, Shapiro-Wilk's and Levene's tests were respectively employed. For comparisons among multiple groups, one-way ANOVA was carried out, followed by Tukey's post hoc test. All statistical analyses were carried out using GraphPad Prism (version 9.0; Dotmatics). $P<0.05$ was considered to indicate a statistically significant difference.

Results

AKG supplementation improves LV remodeling and cardiac dysfunction in LPS-induced septic cardiomyopathy. In the present study, the cardiotoxic effects of LPS in wild-type mice were investigated, focusing on LPS-induced cardiac dysfunction and LV remodeling. Echocardiographic assessments were carried out following exposure to vehicle control, AKG, LPS or a combination of AKG and LPS. Notably, the LV ejection fraction (LVEF) and LV fractional shortening (LVFS) in the LPS group were reduced by 33 and 32%, respectively, compared with those in the control group. Concurrently, there was a 40 and 60% increase in LVEDD and LVESD (Fig. 1A and B). These findings indicated cardiac dysfunction characteristic of septic cardiomyopathy induced by LPS.

The cardioprotective effect of AKG supplementation was evident. AKG treatment led to a 22 and 21% improvement in LVEF and LVFS, along with a 20 and 32% reduction in LVEDD and LVESD, respectively, compared with the LPS group (Fig. 1A and B). There were no significant differences in the cardiac function indices between the AKG group and the control group. This suggested that AKG supplementation did not affect cardiac function when administered alone (Fig. 1B).

Cardiomyocyte remodeling was evaluated by assessing the protein and transcriptional levels of ANP, BNP and β-MHC in the LV myocardium. LPS-treated mice exhibited a notable increase in the mRNA and protein expression levels of these markers, indicative of cardiomyocyte remodeling. However, AKG supplementation may partially mitigate the LPS-induced remodeling (Fig. 1C).

As shown in Fig. S1, the circulating AKG concentration was decreased in the LPS group compared with that in the control group, but the difference was not significant. Although the concentration of circulating AKG increased following AKG supplementation in the LPS group, the differences were not statistically significant.

AKG exposure reverses mitochondrial morphological damage and facilitates mitophagy and fission in LPS-treated mice. Given that mitochondria constitute ~35% of the volume of cardiomyocytes and serve a key role in cellular function (11), a detailed analysis of mitochondrial ultrastructure was performed in heart tissues from mice in the different groups using TEM. LPS treatment induced notable mitochondrial morphological damage, evidenced by increased proportions of mitochondria with incomplete outer membranes or dissolved cristae, compared with those in hearts from the control group (Fig. 2A and B). Additionally, quantitative TEM analysis revealed a reduction in the mitochondrial number. This was further corroborated by assessing the protein levels of Ndufa12 and Ndufab1, which serve as mitochondrial markers (Fig. 2A-C).

Mitochondrial quality control, encompassing processes such as biosynthesis, fusion, fission and mitophagy, is essential for maintaining mitochondrial integrity (11). In hearts from the group subjected to LPS, there was a marked decrease in the expression levels of proteins indicative of mitochondrial

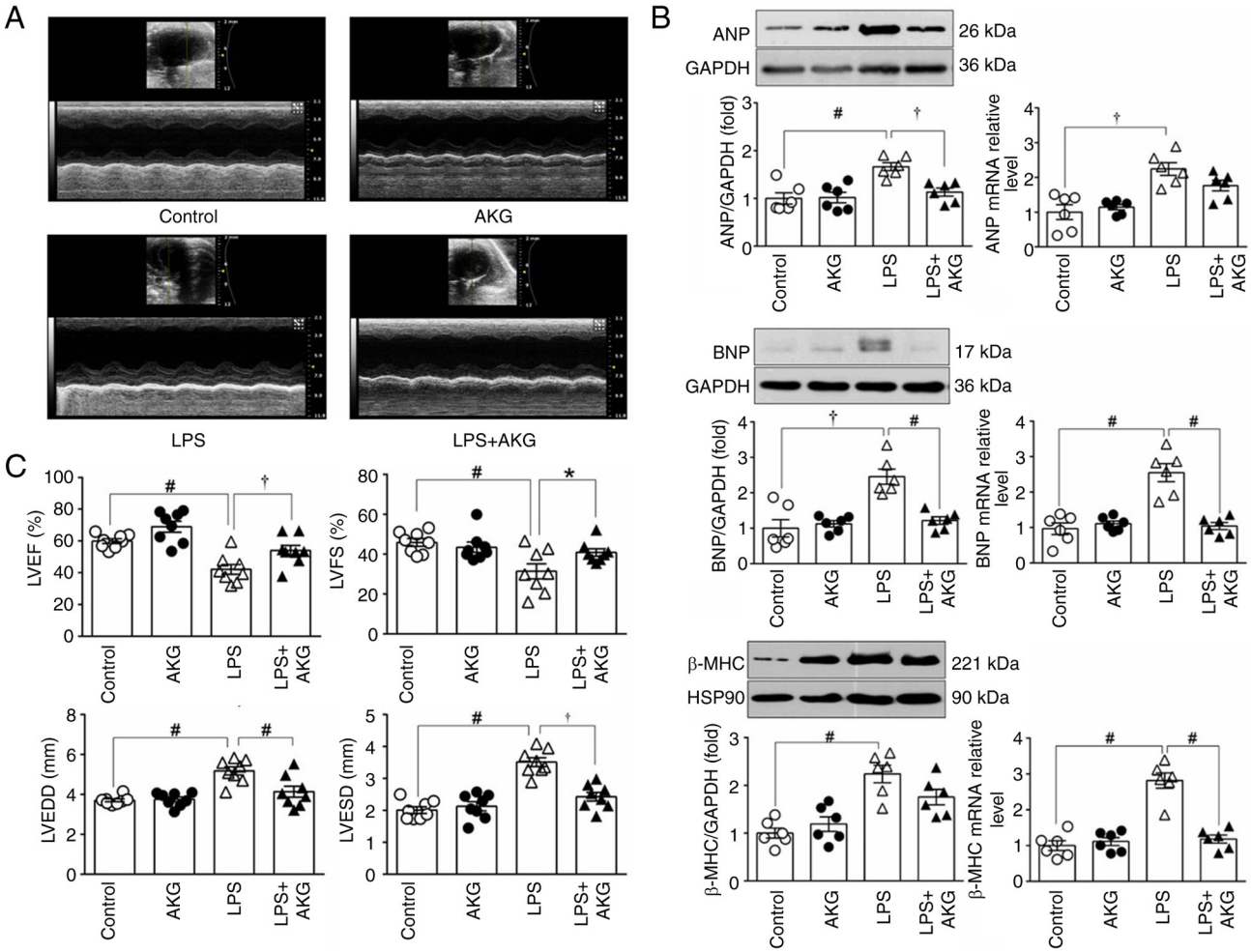

Figure 1. AKG improves cardiac dysfunction in an LPS-induced mouse model of septic cardiomyopathy. (A) Representative 2D echocardiographic images of the LV short-axis from mice treated with control, AKG, LPS and AKG + LPS. (C) LVEF, LVFS, LVEDD and LVESD based on the LV ultrasound images (n=8/group). (B) Protein and mRNA expression levels of ANP, BNP and β-MHC in LV myocardium (n=6/group), GAPDH was used as the loading control for ANP and BNP, while HSP90 was used as the loading control for β-MHC. Data are presented as the mean ± SEM. *P<0.05, †P<0.01, #P<0.001. AKG, α-ketoglutarate; LPS, lipopolysaccharide; LV, left ventricle; LVEF, LV ejection fraction; LVFS, LV fractional shortening; LVEDD, LV end-diastolic dimension; LVESD, LV end-systolic dimension; ANP, atrial natriuretic peptide; BNP, brain natriuretic peptide; β-MHC, β-major histocompatibility complex; HSP90, heat shock protein 90.

fission (DRP1 and Fis1) and mitophagy (LC3 II/I and Bnip3) compared with the control group (Fig. 2C). These findings suggested impaired mitochondrial quality control mechanisms following LPS exposure.

By contrast, AKG treatment mitigated these adverse effects. It restored mitochondrial morphology by reducing the fraction of mitochondria with structural impairments, and increased the overall mitochondrial count, as evidenced by the increased expression levels of mitochondrial content markers (Ndufa12; Fig. 2A-C). Furthermore, AKG positively influenced mitochondrial quality control, demonstrated by the upregulated expression levels of proteins associated with mitochondrial fission and mitophagy (Fig. 2C). This suggested that AKG supplementation counteracted the mitochondrial dysfunction observed in LPS-induced cardiomyopathy.

AKG restores myocardial mitochondrial energy metabolism in septic mice. Generation of ATP through OXPHOS is the primary role of mitochondria and this was further investigated in the context of LPS-induced mitochondrial damage (13). Specifically, the changes in mitochondrial energy metabolism in mouse hearts treated with LPS were assessed.

Initially, immunoblotting was used to analyze heart samples for the presence of specific marker proteins. These included proteins associated with mitochondrial respiratory electron transport chain complexes I, II and IV (MT-ND1, SDHA and COX IV), and key enzymes involved in acetyl-CoA production and the TCA cycle (PDH and OGDH). A notable decrease in the expression levels of these proteins was observed, indicating impaired mitochondrial aerobic oxidation. Conversely, the protein levels of HIF-1α, indicative of anaerobic glycolysis, were revealed to be elevated following LPS treatment (Fig. 3A and B).

Furthermore, to directly assess mitochondrial functionality, the levels of ATP and lactate were measured using an ELISA. Analysis revealed a significant reduction in ATP levels in the hearts of mice treated with LPS, accompanied by an increase in lactate content in LV tissues and plasma (Fig. 3C). AKG supplementation led to a partial increase in the abundance of proteins associated with aerobic oxidation

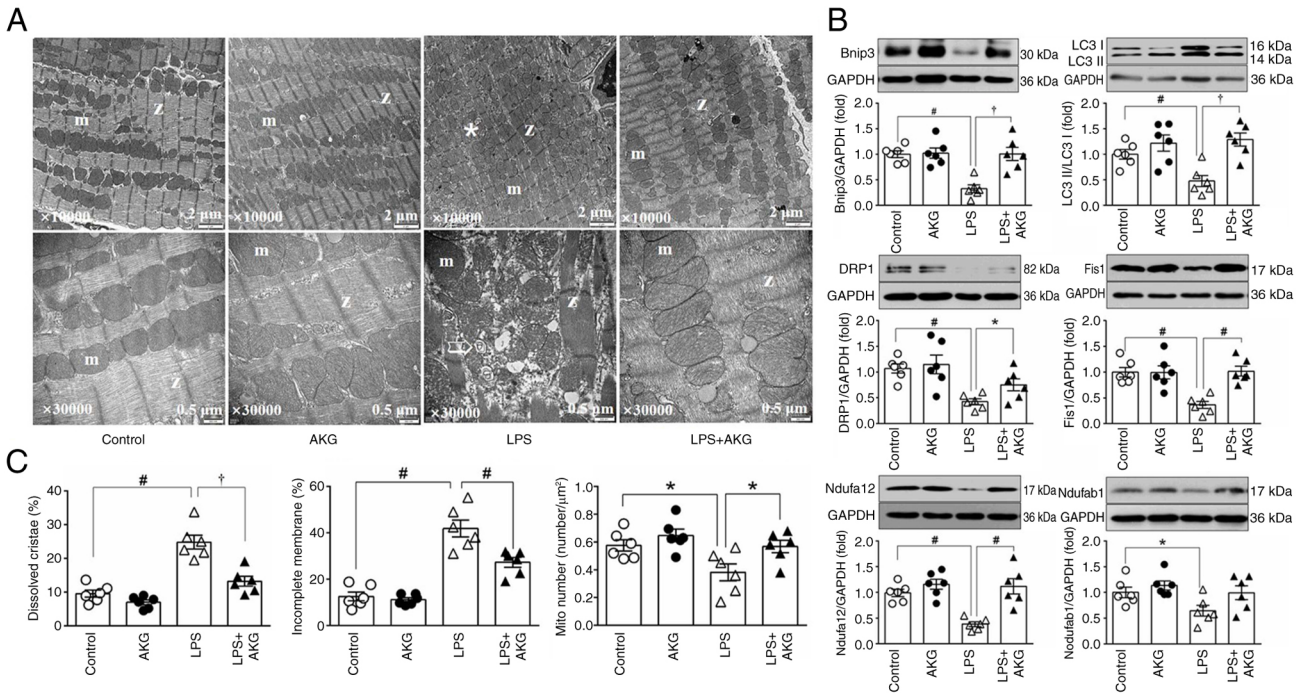

Figure 2. AKG alleviates myocardial mitochondrial morphological damage induced by LPS. (A) Electron microscopy images of left ventricular myocardium. Magnification: Top, x10,000; bottom, x30,000. *Mitochondria with dissolved cristae; the arrow indicates mitochondria with incomplete outer membranes (n=6/group). (B) Representative immunoblotting images and semi-quantitative analysis of protein expression of markers of mitochondrial mitophagy (Bnip3 and LC3), fission (DRP1 and Fis1) and mitochondrial content (Ndufab1 and Ndufa12; n=6/group). (C) Quantitative analysis of mitochondria. The percentage of mitochondria with an incomplete outer membrane and dissolved cristae, and the number of mitochondria per unit area (n=6/group). Data are presented as the mean ± SEM. *P<0.05, †P<0.01, #P<0.001. AKG, α-ketoglutarate; m, mitochondria; Z, Z line; Mito number, the number of mitochondria per unit area; Bnip3, BCL2 interacting protein 3; DRP1, dynamin-related protein 1; Ndufa, NADH:ubiquinone oxidoreductase subunits; LPS, lipopolysaccharide.

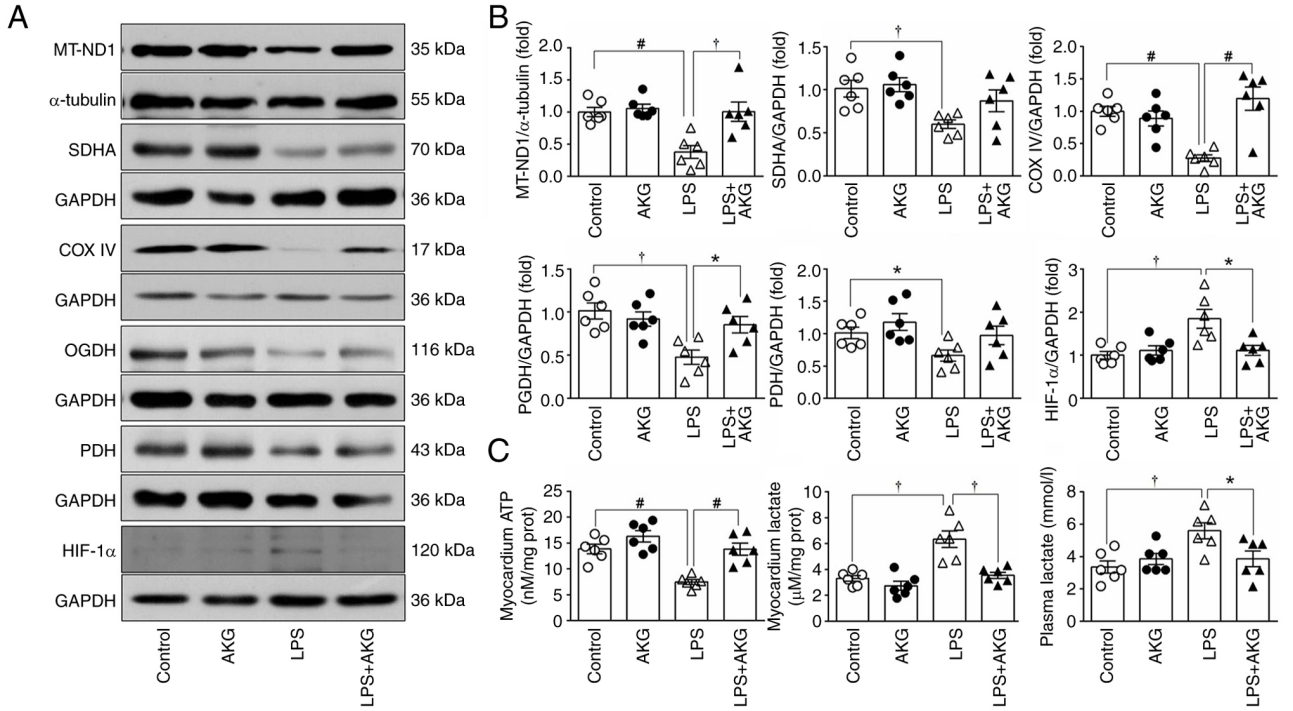

Figure 3. AKG recovers myocardial mitochondrial energy metabolism in an LPS-induced mouse model of septic cardiomyopathy. Western blotting was carried out using protein extracted from LV tissues, and protein expression was semi-quantified and normalized to GAPDH (n=6/group). (A) Representative blots of marker proteins for mitochondrial energy metabolism: Mitochondrial complex I (MT-ND1), complex II (SDHA), COX IV, tricarboxylic acid cycle (OGDH), a key enzyme for acetyl-CoA synthesis (PDH) and anaerobic glycolysis (HIF-1α). (B) Semi-quantitative analysis of mitochondrial energy metabolism marker proteins. (C) ATP content in the LV tissues, and lactate content in the plasma and LV tissues, as determined by an ELISA (n=6/group). Data are presented as the mean ± SEM. *P<0.05, †P<0.01, #P<0.001. LV, left ventricle; MT-ND1, mitochondrial NADH-ubiquinone oxidoreductase chain 1; HIF-1α, hypoxia inducible factor-1α; OGDH, ketoglutarate dehydrogenase; PDH, pyruvate dehydrogenase; SDHA, succinate dehydrogenase; AKG, α-ketoglutarate; LPS, lipopolysaccharide; COX IV, complex IV; prot, protein.

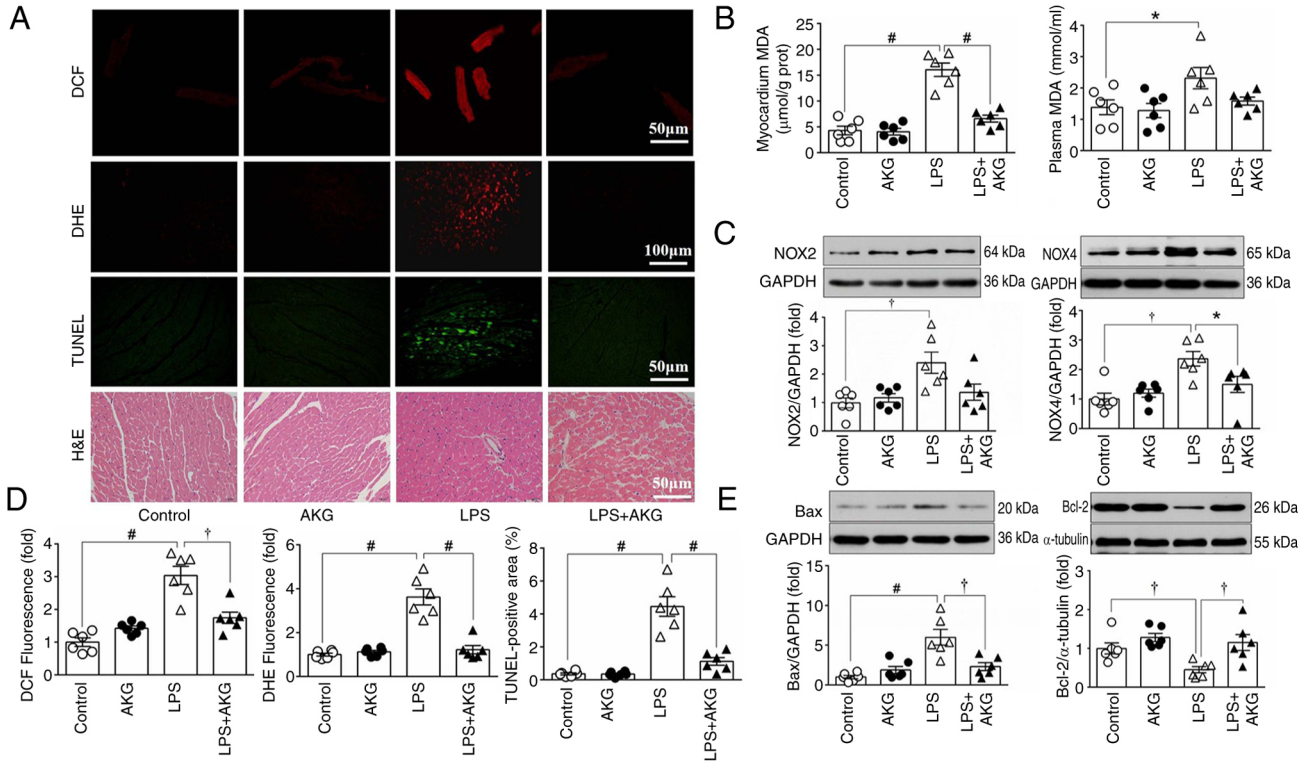

Figure 4. AKG reduces myocardial ROS and apoptosis in an LPS-induced mouse model of septic cardiomyopathy. ROS levels were detected using various methods, including DCF staining, DHE staining, MDA content determination using an ELISA, and examination of NOX2/4 protein expression. Apoptosis was assessed via TUNEL staining, and examination of the protein expression levels of Bax and Bcl-2. (A) From top to bottom: Representative images of DCF, DHE, TUNEL and H&E staining (n=6/group). (B) Changes in myocardial and plasma levels of MDA (n=6/group). (C) Western blot bands and analysis of marker proteins for NOX2 and NOX4 (n=6/group). (D) Quantitative analysis of DCF, DHE and TUNEL staining (n=6/group). (E) Representative blots and analysis of marker proteins for Bax and Bcl-2 (n=6/group). Data are presented as the mean ± SEM. *P<0.05, †P<0.01, $^{\#}$P<0.001. AKG, α-ketoglutarate; LPS, lipopolysaccharide; ROS, reactive oxygen species; DCF, chloromethyl derivative CM-H_2DCFDA; DHE, dihydroethidium; MDA, malondialdehyde; NOX, NADPH oxidase; prot, protein.

and ATP production, while concurrently decreasing the levels of HIF-1α and lactate (Fig. 3A-C). This suggested that AKG reversed the alterations in mitochondrial energy metabolism induced by LPS treatment.

AKG reduces ROS content and inhibits apoptosis in mice treated with LPS. Given the key role of mitochondria in the regulation of ROS generation and apoptosis (15), the impact of AKG on these parameters in LPS-induced cardiomyopathy was assessed.

To assess oxidative stress, DCF and DHE staining were carried out to determine ROS levels in myocardial tissue (Fig. 4A and B). Additionally, the expression levels of key enzymes involved in ROS production, namely NOX2 and NOX4, were examined (Fig. 4D). MDA, a biomarker of lipid peroxidation, was also measured to provide further insights into oxidative stress (Fig. 4C). Compared with the control group, a significant increase in ROS generation was observed in the LPS-treated group. This elevation in ROS levels was mitigated in the LPS + AKG group, suggesting that AKG reduced oxidative stress in LPS-induced septic cardiomyopathy.

To evaluate apoptosis, TUNEL staining was performed and the protein expression levels of Bax and Bcl-2 in myocardial tissue were measured. Enhanced apoptosis was evident in the LPS group compared with both the control and AKG groups (Fig. 4A, B and E). However, AKG administration in the LPS-treated group led to a reduction in apoptosis. These findings indicated that AKG supplementation attenuated both oxidative stress and apoptosis induced by LPS in the context of septic cardiomyopathy.

To examine the morphology of the myocardium, H&E staining was performed. In the LPS group, the myocardium showed a disorderly arrangement of myocytes, karyolysis and an increased presence of inflammatory cells. However, AKG administration improved the abnormal histological structure (Fig. 4A).

AKG reduces apoptosis, improves mitochondrial energy metabolism and increases mitochondrial turnover in vitro. The effects of AKG on NRVMs subjected to LPS treatment were explored (Fig. 5). The impact on apoptosis was initially assessed using TUNEL staining and measurement of Bcl-2 protein levels. Compared with the control group, a seven-fold increase in the optical density of TUNEL-positive cells was observed in the LPS group, coupled with a significant decrease in Bcl-2 protein levels, indicating increased apoptosis due to LPS exposure. However, simultaneous administration of AKG significantly mitigated LPS-induced apoptosis in NRVMs (Fig. 5A, D and E).

Additionally, the expression levels of marker proteins integral to mitochondrial aerobic oxidation, including MT-ND1, SDHA, COX IV, OGDH and PDH, were explored. LPS

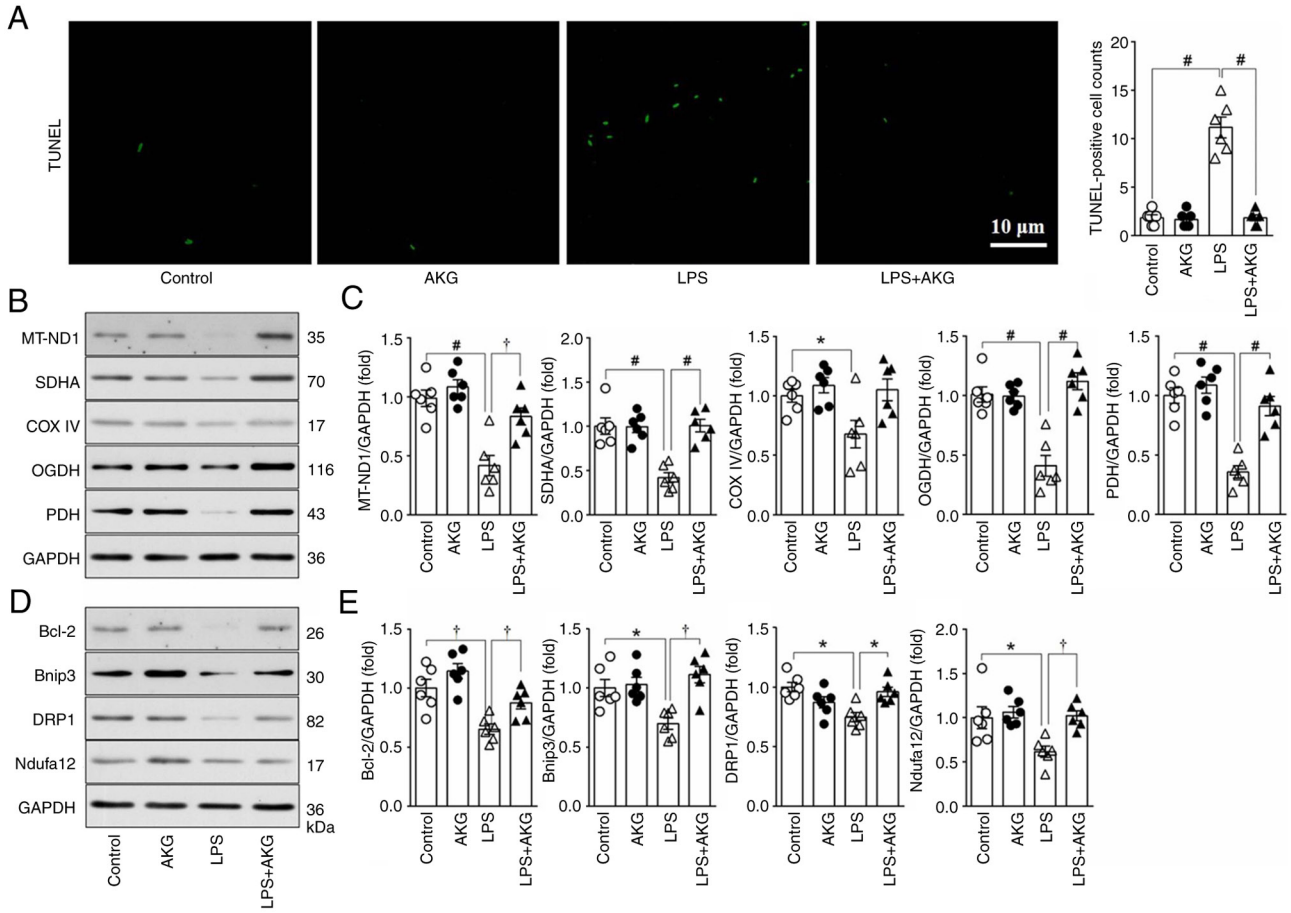

Figure 5. Effect of AKG on apoptosis and mitochondrial metabolism and dynamics *in vitro*. Neonatal rat ventricular myocytes were treated with vehicle, AKG, LPS or AKG + LPS. (A) Images and quantitative analysis of the TUNEL staining (n=6/group). (B) Representative western blot images and (C) semi-quantification of markers for mitochondrial metabolism (MT-ND1, SDHA, COX IV, OGDH and PDH) (n=6/group). (D) Protein expression levels of selected markers for apoptosis (Bcl-2), mitochondrial quality control (Bnip3 and DRP1) and mitochondrial number (Ndufa12). (E) Semi-quantitative analysis of protein expression of Bcl-2, Bnip3, DRP1 and Ndufa12) (n=6/group). Data are presented as the mean ± SEM. *P<0.05, †P<0.01, $^{\#}$P<0.001. AKG, α-ketoglutarate; LPS, lipopolysaccharide; MT-ND1, mitochondrial NADH-ubiquinone oxidoreductase chain 1; SDHA, succinate dehydrogenase; COX IV, complex IV; OGDH, ketoglutarate dehydrogenase; PDH, pyruvate dehydrogenase; Bnip3, BCL2 interacting protein 3; DRP1, dynamin-related protein 1; Nduf, NADH:ubiquinone oxidoreductase subunits.

treatment resulted in a significant reduction in the expression levels of these proteins. By contrast, AKG administration alleviated this reduction, suggesting its efficacy in improving mitochondrial aerobic oxidation when this is compromised by LPS (Fig. 5B and C).

Immunoblotting analysis revealed alterations in mitochondrial turnover induced by LPS, evidenced by decreased expression levels of proteins associated with mitophagy (Bnip3) and fission (DRP1), along with a reduction in the mitochondrial content marker Ndufa12. Notably, AKG supplementation significantly counteracted these effects, suggesting its potential to restore mitochondrial turnover disrupted by LPS treatment (Fig. 5D and E). These findings collectively underscore the therapeutic potential of AKG in mitigating mitochondrial dysfunction and apoptosis in LPS-induced cardiomyopathy.

AKG improves mitochondrial respiration damage induced by LPS in vitro. Whether AKG directly enhanced mitochondrial function was subsequently assessed. A Seahorse XF mitochondrial stress test analyzer was used to evaluate the mitochondrial respiratory capacity in NRVMs (Fig. 6A).

Key parameters of mitochondrial respiratory function, including basal and maximal respiratory capacity (Fig. 6C and D), ATP production (Fig. 6E) and spare respiratory capacity (Fig. 6G), were assessed. These parameters were found to be significantly compromised in NRVMs treated with LPS, compared with those in the control group. Notably, when AKG was administered in conjunction with LPS, an improvement in mitochondrial respiration was observed.

This enhancement suggested that AKG supplementation effectively counteracted the mitochondrial dysfunction induced by LPS in NRVMs. In the present study, no significant differences in non-mitochondrial respiration in NRVMs were observed.

Discussion

In the present study, focusing on the mechanism of myocardial mitochondrial damage in septic cardiomyopathy, NRVMs and animal models were used to investigate the effects of AKG supplementation on LPS-induced myocardial injury. The results revealed several novel insights: Firstly, LPS was revealed to mediate cardiac remodeling

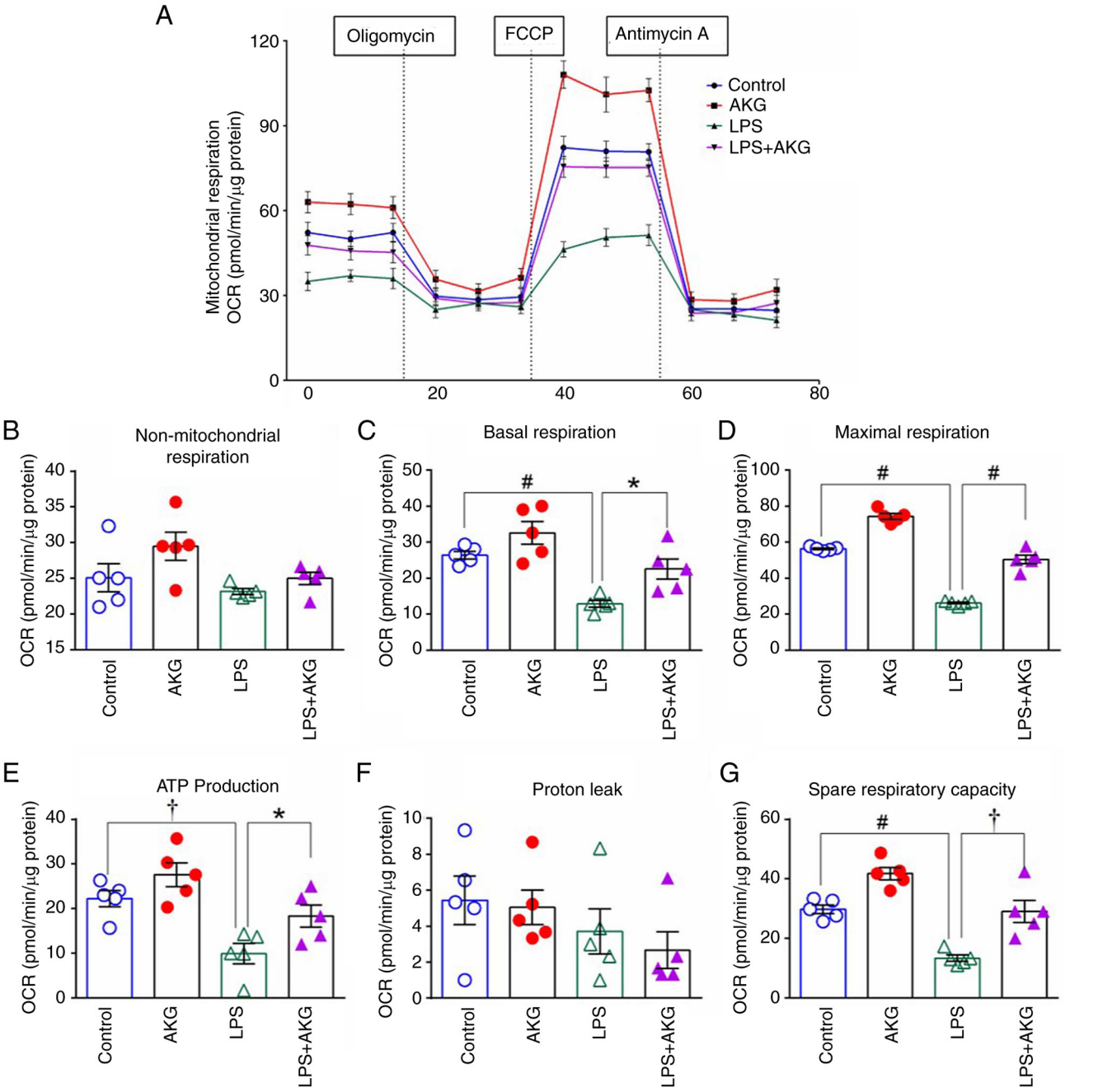

Figure 6. Effect of AKG on mitochondrial respiratory capacity *in vitro*. (A) OCR curve of the control, AKG, LPS and AKG + LPS groups (n=5/group). (B) Non-mitochondrial respiration, (C) basal respiration, (D) maximal respiration, (E) ATP production, (F) proton leak and (G) spare respiration capacity were calculated. Data are presented as the mean ± SEM. *P<0.05, †P<0.01, $^{\#}$P<0.001. AKG, α-ketoglutarate; LPS, lipopolysaccharide; OCR, oxygen consumption rate; FCCP, trifluoromethoxy carbonylcyanide phenylhydrazone.

and dysfunction; secondly, myocardial mitochondrial damage in septic cardiomyopathy, as evidenced by morphological abnormalities, impaired mitochondrial quality control and reduced energy metabolism, was accompanied by increased apoptosis and ROS production; and thirdly, the present study demonstrated that AKG supplementation alleviated myocardial mitochondrial damage and improved cardiac function in septic cardiomyopathy. The present results highlight the therapeutic potential of AKG in mitigating mitochondrial dysfunction and associated cardiac impairments in this condition, providing a possible direction for future research and treatment approaches.

AKG, a key intermediate of the Krebs cycle, situated between succinyl CoA and isocitrate, serves as a precursor for glutamate and glutamine (32). Notably, circulating AKG levels are elevated in patients with heart failure, but are decreased in obese and diabetic individuals (32,33). Previous animal research has indicated a reduction in AKG levels in diabetic cardiomyopathy and ischemic heart failure (34), and supplementation with AKG ameliorated myocardial pathological remodeling and enhanced cardiac function in these models (22,23). Despite these findings, to the best of our knowledge, the specific role of AKG in septic cardiomyopathy remains unexplored. The present study addresses this gap by

investigating the impact of AKG in septic cardiomyopathy induced by LPS, shedding light on potential therapeutic avenues in this context.

The present study demonstrated that AKG supplementation mitigated cardiac dysfunction induced by LPS, as evidenced by echocardiographic assessments. Furthermore, myocardial remodeling was assessed based on the mRNA and protein expression levels of ANP, BNP and β-MHC, which revealed that AKG effectively reduced pathological myocardial remodeling. However, the precise mechanism by which AKG improved cardiac function remains unclear. Our previous studies investigated mitochondrial damage mechanisms in dilated cardiomyopathy (24), takotsubo cardiomyopathy (25) and antitumor drug-induced cardiomyopathy (26). Notably, mitochondrial abnormalities have been recognized as a pivotal factor in the pathogenesis of septic cardiomyopathy (7). Building upon this understanding, the role of mitochondrial damage mechanisms in septic cardiomyopathy and the therapeutic efficacy of AKG were assessed.

In the present study, exploration of mitochondrial morphology in septic cardiomyopathy using TEM revealed abnormal mitochondrial ultrastructure in the myocardium from mice exposed to LPS, notably characterized by an increased proportion of mitochondria with incomplete outer membranes and dissolved cristae. This structural damage facilitates the release of mitochondrial DNA into the cytoplasm, exacerbating myocardial damage and systemic inflammation (35). Additionally, such compromised mitochondria may prompt the cytoplasmic release of pro-apoptotic proteins such as cytochrome *c*, further promoting apoptosis (36,37). Mitochondria are subject to rigorous 'quality control' processes, including biosynthesis, fission, fusion and mitophagy, to maintain their quality and quantity (38). In the present study, a reduction in the expression levels of proteins associated with mitochondrial fission and mitophagy was observed, which was consistent with the decreased mitochondrial count detected by electron microscopy. While moderate mitophagy and fission are key for clearing damaged mitochondria and ensuring ATP production (39), their insufficiency leads to an accumulation of dysfunctional mitochondria. Of note, the findings of the present study indicated that AKG supplementation counteracted these detrimental changes. Both TEM and biochemical assays suggested that AKG enhanced mitochondrial quality control, facilitating the elimination of damaged and malfunctioning mitochondria and thereby sustaining mitochondrial self-renewal and function.

To investigate the impact of mitochondrial morphological changes on the function of mitochondria, the present study assessed mitochondrial function in septic cardiomyopathy. Mitochondria primarily generate ATP through OXPHOS (13). LPS exposure reduced the levels of marker proteins for mitochondrial electron transport chain complexes (MT-ND1, SDHA and COX IV) and key enzymes of the mitochondrial TCA cycle (OGDH) and acetyl CoA synthesis (PDH), which are key for mitochondrial aerobic oxidation. Correspondingly, there was a noticeable decrease in ATP levels in the myocardium exposed to LPS, in agreement with other findings in septic cardiomyopathy (8). Furthermore, an increase in lactate levels in myocardium and plasma, along with an increase in HIF-1α protein levels, indicated a shift towards anaerobic glycolysis while inhibiting OXPHOS (40). Notably, AKG supplementation effectively reversed these disturbances in mitochondrial energy metabolism. In addition, mitochondrial function was indirectly evaluated by measuring ROS levels and apoptosis in myocardial tissues. Mitochondria are considerable producers of ROS, especially during OXPHOS, with 11 potential ROS-generating sites, particularly in complexes I and III (41). LPS treatment led to an increase in myocardial ROS abundance and enhanced apoptosis. By contrast, AKG supplementation significantly mitigated these pathological changes, as evidenced by DCF, DHE and TUNEL staining, along with the assessment of oxidative stress (MDA and NOX2/4) and apoptosis-related proteins (Bax and Bcl-2). There was no significant change in the expression of MDA in the plasma after AKG administration, which might be influenced by the metabolism of other organs. These results collectively suggested that AKG effectively alleviated the dysfunction of myocardial mitochondria in LPS-induced septic cardiomyopathy.

In an extension of the *in vivo* research, *in vitro* experiments were performed to further elucidate the effects of LPS and AKG supplementation on mitochondrial function in NRVMs. In agreement with the results of the animal studies, exposure of NRVMs to LPS resulted in increased apoptosis and a reduction in the expression levels of proteins that are key for mitochondrial aerobic oxidation and mitochondrial quality control. Conversely, AKG supplementation effectively reversed these detrimental effects. Analysis of the Seahorse metabolic flux analyzer data demonstrated that AKG administration significantly ameliorated LPS-induced disturbances in mitochondrial respiratory capacity. This improvement was evidenced by the normalization of key parameters such as basal respiration, maximal respiration and ATP production, underscoring the potential of AKG in mitigating mitochondrial dysfunction in septic cardiomyopathy.

A limitation of the present study is that it primarily focused on the effects of short-term administration of AKG, but the long-term effects and potential side effects of AKG administration were not fully investigated. Another limitation is that although the present study supported the protective effect of AKG in septic cardiomyopathy induced by LPS, the precise molecular mechanisms underlying these beneficial effects were not fully elucidated. In addition, the present study investigated the effects of AKG in male mice only; its effect in female mice was not assessed.

In summary, the present study on LPS-induced septic cardiomyopathy revealed that AKG supplementation enhanced cardiac performance and rectified cardiac dysfunction. This effect was achieved through restoration of mitochondrial ultrastructure, augmentation of energy metabolism, and reduction of oxidative stress and cellular apoptosis. The present study not only shed light on the underlying mechanisms of myocardial mitochondrial damage in septic cardiomyopathy but also suggested that AKG-based therapeutic interventions may be a treatment option for this condition. Thus, these findings offer insights and pave the way for the development of novel AKG-based therapeutic strategies in the management of septic cardiomyopathy.

Acknowledgements

Not applicable.

Funding

The present study was funded by grants from the Key Research and Development of Shaanxi Province (grant no. 2021ZDLSF02-03), the National Natural Scientific Foundation of China (grant no. 82070858), the Youth Scientific Research and Innovation Team Program of Shaanxi Province (grant no. 2022-SLRH-LJ-014), and the Technology Talents Support Program of Shaanxi Provincial People's Hospital (grant no. 2023JY-28).

Availability of data and materials

The data generated in the present study may be requested from the corresponding author.

Authors' contributions

WW, BYX, JKW, GCG and ZWL conceived and designed the experiments and wrote the manuscript. WW, BYX, QM, SS and BTL performed the experiments and analyzed the data. ZWL, SS and JKW made substantial contributions to manuscript revision and supervision. WW, BYX and GCG confirm the authenticity of all the raw data. All authors have read and approved the final version of the manuscript.

Ethics approval and consent to participate

The animal experiments were approved by the Ethical Committee of Shaanxi Provincial People's Hospital (approval no. 2021071; Xi'an, China).

Patient consent for publication

Not applicable.

Competing interests

The authors declare that they have no competing interests.

References

1. Singer M, Deutschman CS, Seymour CW, Shankar-Hari M, Annane D, Bauer M, Bellomo R, Bernard GR, Chiche JD, Coopersmith CM, *et al*: The third international consensus definitions for sepsis and septic shock (sepsis-3). JAMA 315: 801-810, 2016.
2. Fleischmann C, Scherag A, Adhikari NK, Hartog CS, Tsaganos T, Schlattmann P, Angus DC and Reinhart K; International Forum of Acute Care Trialists: Assessment of global incidence and mortality of hospital-treated sepsis. Current estimates and limitations. Am J Respir Crit Care Med 193: 259-272, 2016.
3. Prescott HC and Angus DC: Enhancing recovery from sepsis: A review. JAMA 319: 62-75, 2018.
4. Sato R and Nasu M: A review of sepsis-induced cardiomyopathy. J Intensive Care 3: 48, 2015.
5. Hollenberg SM and Singer M: Pathophysiology of sepsis-induced cardiomyopathy. Nat Rev Cardiol 18: 424-434, 2021.
6. van der Poll T, van de Veerdonk FL, Scicluna BP and Netea MG: The immunopathology of sepsis and potential therapeutic targets. Nat Rev Immunol 17: 407-420, 2017.
7. Haileselassie B, Mukherjee R, Joshi AU, Napier BA, Massis LM, Ostberg NP, Queliconi BB, Monack D, Bernstein D and Mochly-Rosen D: Drp1/Fis1 interaction mediates mitochondrial dysfunction in septic cardiomyopathy. J Mol Cell Cardiol 130: 160-169, 2019.
8. Zhu XX, Wang X, Jiao SY, Liu Y, Shi L, Xu Q, Wang JJ, Chen YE, Zhang Q, Song YT, *et al*: Cardiomyocyte peroxisome proliferator-activated receptor α prevents septic cardiomyopathy via improving mitochondrial function. Acta Pharmacol Sin 44: 2184-2200, 2023.
9. Kong W, Kang K, Gao Y, Liu H, Meng X, Yang S, Yu K and Zhao M: Dexmedetomidine alleviates LPS-induced septic cardiomyopathy via the cholinergic anti-inflammatory pathway in mice. Am J Transl Res 9: 5040-5047, 2017.
10. Brealey D, Brand M, Hargreaves I, Heales S, Land J, Smolenski R, Davies NA, Cooper CE and Singer M: Association between mitochondrial dysfunction and severity and outcome of septic shock. Lancet 360: 219-223, 2002.
11. Dorn GW II: Mitochondrial dynamics in heart disease. Biochim Biophys Acta 1833: 233-241, 2013.
12. Lelubre C and Vincent JL: Mechanisms and treatment of organ failure in sepsis. Nat Rev Nephrol 14: 417-427, 2018.
13. Dorn GW II, Vega RB and Kelly DP: Mitochondrial biogenesis and dynamics in the developing and diseased heart. Genes Dev 29: 1981-1991, 2015.
14. Martínez-Reyes I and Chandel NS: Mitochondrial TCA cycle metabolites control physiology and disease. Nat Commun 11: 102, 2020.
15. Sies H and Jones DP: Reactive oxygen species (ROS) as pleiotropic physiological signalling agents. Nat Rev Mol Cell Biol 21: 363-383, 2020.
16. Mantzarlis K, Tsolaki V and Zakynthinos E: Role of oxidative stress and mitochondrial dysfunction in sepsis and potential therapies. Oxid Med Cell Longev 2017: 5985209, 2017.
17. Carey BW, Finley LW, Cross JR, Allis CD and Thompson CB: Intracellular α-ketoglutarate maintains the pluripotency of embryonic stem cells. Nature 518: 413-416, 2015.
18. Chang LC, Chiang SK, Chen SE and Hung MC: Targeting 2-oxoglutarate dehydrogenase for cancer treatment. Am J Cancer Res 12: 1436-1455, 2022.
19. Asadi Shahmirzadi A, Edgar D, Liao CY, Hsu YM, Lucanic M, Asadi Shahmirzadi A, Wiley CD, Gan G, Kim DE, Kasler HG, *et al*: Alpha-ketoglutarate, an endogenous metabolite, extends lifespan and compresses morbidity in aging mice. Cell Metab 32: 447-456.e6, 2020.
20. TeSlaa T, Chaikovsky AC, Lipchina I, Escobar SL, Hochedlinger K, Huang J, Graeber TG, Braas D and Teitell MA: α-Ketoglutarate accelerates the initial differentiation of primed human pluripotent stem cells. Cell Metab 24: 485-493, 2016.
21. Matzi V, Lindenmann J, Muench A, Greilberger J, Juan H, Wintersteiger R, Maier A and Smolle-Juettner FM: The impact of preoperative micronutrient supplementation in lung surgery. A prospective randomized trial of oral supplementation of combined alpha-ketoglutaric acid and 5-hydroxymethylfurfural. Eur J Cardiothorac Surg 32: 776-782, 2007.
22. Dhat R, Mongad D, Raji S, Arkat S, Mahapatra NR, Singhal N and Sitasawad SL: Epigenetic modifier alpha-ketoglutarate modulates aberrant gene body methylation and hydroxymethylation marks in diabetic heart. Epigenetics Chromatin 16: 12, 2023.
23. An D, Zeng Q, Zhang P, Ma Z, Zhang H, Liu Z, Li J, Ren H and Xu D: Alpha-ketoglutarate ameliorates pressure overload-induced chronic cardiac dysfunction in mice. Redox Biol 46: 102088, 2021.
24. Wu W, Ziemann M, Huynh K, She G, Pang ZD, Zhang Y, Duong T, Kiriazis H, Pu TT, Bai RY, *et al*: Activation of Hippo signaling pathway mediates mitochondria dysfunction and dilated cardiomyopathy in mice. Theranostics 11: 8993-9008, 2021.
25. Wu W, Lu Q, Ma S, Du JC, Huynh K, Duong T, Pang ZD, Donner D, Meikle PJ, Deng XL and Du XJ: Mitochondrial damage in a takotsubo syndrome-like mouse model mediated by activation of β-adrenoceptor-Hippo signaling pathway. Am J Physiol Heart Circ Physiol 324: H528-H541, 2023.
26. She G, Du JC, Wu W, Pu TT, Zhang Y, Bai RY, Zhang Y, Pang ZD, Wang HF, Ren YJ, *et al*: Hippo pathway activation mediates chemotherapy-induced anti-cancer effect and cardiomyopathy through causing mitochondrial damage and dysfunction. Theranostics 13: 560-577, 2023.
27. Abdulmahdi W, Patel D, Rabadi MM, Azar T, Jules E, Lipphardt M, Hashemiyoon R and Ratliff BB: HMGB1 redox during sepsis. Redox Biol 13: 600-607, 2017.

28. McGrath JC and Lilley E: Implementing guidelines on reporting research using animals (ARRIVE etc.): New requirements for publication in BJP. Br J Pharmacol 172: 3189-3193, 2015.
29. Zhao H, Zhang M, Zhou F, Cao W, Bi L, Xie Y, Yang Q and Wang S: Cinnamaldehyde ameliorates LPS-induced cardiac dysfunction via TLR4-NOX4 pathway: The regulation of autophagy and ROS production. J Mol Cell Cardiol 101: 11-24, 2016.
30. Livak KJ and Schmittgen TD: Analysis of relative gene expression data using real-time quantitative PCR and the 2(-Delta Delta C(T)) method. Methods 25: 402-408, 2001.
31. Han Y, Tian H and Gao X: NORAD regulates proliferation and apoptosis in cardiomyocytes under high-glucose treatment through miRNA-150-5p/ZEB1 axis. Eur Rev Med Pharmacol Sci 24: 11259-11265, 2020.
32. Chen PA, Xu ZH, Huang YL, Luo Y, Zhu DJ, Wang P, Du ZY, Yang Y, Wu DH, Lai WY, *et al*: Increased serum 2-oxoglutarate associated with high myocardial energy expenditure and poor prognosis in chronic heart failure patients. Biochim Biophys Acta 1842: 2120-2125, 2014.
33. Spallotta F, Cencioni C, Atlante S, Garella D, Cocco M, Mori M, Mastrocola R, Kuenne C, Guenther S, Nanni S, *et al*: Stable oxidative cytosine modifications accumulate in cardiac mesenchymal cells from type2 diabetes patients: Rescue by α-ketoglutarate and TET-TDG functional reactivation. Circ Res 122: 31-46, 2018.
34. Lai L, Leone TC, Keller MP, Martin OJ, Broman AT, Nigro J, Kapoor K, Koves TR, Stevens R, Ilkayeva OR, *et al*: Energy metabolic reprogramming in the hypertrophied and early stage failing heart: a multisystems approach. Circ Heart Fail 7: 1022-1031, 2014.
35. Yan C, Duanmu X, Zeng L, Liu B and Song Z: Mitochondrial DNA: Distribution, mutations, and elimination. Cells 8: 379, 2019.
36. Galluzzi L, Vitale I, Aaronson SA, Abrams JM, Adam D, Agostinis P, Alnemri ES, Altucci L, Amelio I, Andrews DW, *et al*: Molecular mechanisms of cell death: Recommendations of the nomenclature committee on cell death 2018. Cell Death Differ 25: 486-541, 2018.
37. Ghezzi D, Sevrioukova I, Invernizzi F, Lamperti C, Mora M, D'Adamo P, Novara F, Zuffardi O, Uziel G and Zeviani M: Severe X-linked mitochondrial encephalomyopathy associated with a mutation in apoptosis-inducing factor. Am J Hum Genet 86: 639-649, 2010.
38. Tilokani L, Nagashima S, Paupe V and Prudent J: Mitochondrial dynamics: Overview of molecular mechanisms. Essays Biochem 62: 341-360, 2018.
39. Chaanine AH, Joyce LD, Stulak JM, Maltais S, Joyce DL, Dearani JA, Klaus K, Nair KS, Hajjar RJ and Redfield MM: Mitochondrial morphology, dynamics, and function in human pressure overload or ischemic heart disease with preserved or reduced ejection fraction. Circ Heart Fail 12: e005131, 2019.
40. Shirihai OS, Song M and Dorn GW II: How mitochondrial dynamism orchestrates mitophagy. Circ Res 116: 1835-1849, 2015.
41. Brand MD: Mitochondrial generation of superoxide and hydrogen peroxide as the source of mitochondrial redox signaling. Free Radic Biol Med 100: 14-31, 2016.